



# Multi-level radioisotope batteries based on $^{60}\text{Co}$ $\gamma$ source and Radio-voltaic/Radio-photovoltaic dual effects

Xiao Guo<sup>a</sup>, Yunpeng Liu<sup>a,b</sup>, Zhiheng Xu<sup>a</sup>, Zhangang Jin<sup>a</sup>, Kai Liu<sup>a</sup>, Zicheng Yuan<sup>a</sup>, Pin Gong<sup>a,b</sup>, Xiaobin Tang<sup>a,b,\*</sup>

<sup>a</sup> Department of Nuclear Science and Engineering, Nanjing University of Aeronautics and Astronautics, 29 Yuda St., Nanjing 210016, China

<sup>b</sup> Jiangsu Key Laboratory of Material and Technology for Energy Conversion, 29 Yuda St., Nanjing 210016, China



## ARTICLE INFO

### Article history:

Received 14 February 2018

Received in revised form 2 April 2018

Accepted 7 April 2018

Available online 9 April 2018

### Keywords:

Radio-voltaic/radio-photovoltaic dual effect

Multi-Level isotope battery

$^{60}\text{Co}$   $\gamma$  source

MCNP5

## ABSTRACT

A dual effect multi-level isotope battery based on  $\gamma$  radioisotope source was proposed. Two types of energy conversion mechanisms, namely, radio-voltaic (RV) and radio-photovoltaic (RPV) effects, was combined to convert the radiation energy of  $\gamma$  ray to electricity. The theoretical performance limit for the dual effect multi-level isotope battery irradiated by  $^{60}\text{Co}$  radioisotope source was calculated, and the characteristics of each conversion mechanism were analyzed by using MCNP5. The results revealed that the RPV effect produced more electrical output than the RV effect, but the contribution of each effect on the battery was significant. The output performance of the multi-level isotope battery was characterized under  $^{60}\text{Co}$  source at dose rates of 0.103 kGy/h and 0.68 kGy/h. The theoretical and experimental study investigated the feasibility of combining two kinds of energy conversion mechanisms to enhance the performance of nuclear batteries. The use of  $^{60}\text{Co}$  radioisotope sources with a large activity and conversion modules with additional levels could obtain a considerable output performance. Moreover, the thickness influence of the LYSO scintillator on the performance limit in the first-level conversion module was studied to optimize the structural parameters of the multi-level dual effect isotope battery. The thickness of scintillator strongly affects the energy deposition distribution of gamma rays in the multi-level conversion module, resulting in changes of the output generated by RV and RPV effects, which in turn affects the total output of the battery.

© 2018 Elsevier B.V. All rights reserved.

## 1. Introduction

With the development of the military, aerospace, biomedicine, providing a stable and independent energy supply for the electronic modules used in these fields has become a key concern that needs an urgent solution. Radio-voltaic (RV) and radio-photovoltaic (RPV) radioisotope batteries have huge potential application values for their advantage of high power density, long life, and ultraminiature size. The RV radioisotope battery is based on the direct action of the ray and the energy conversion module to produce an electrical output, which is a direct energy conversion mechanism. The RPV nuclear battery is an indirect energy conversion mechanism that converts decay energy into light energy and then into electricity. With the advances in semiconductor processing technology, some progress has been achieved in RV and RPV radioisotope bat-

tery. Research on RV radioisotope battery focused on the structural design of the energy conversion unit [1–3] and the development of a new type of conversion material [4–6], which achieved a certain progress. However, high energy particles are prone to make lattice damage in the semiconductor conversion modules, resulting in a rapid decline in battery performance [7]. Therefore, using high energy  $\alpha$  or  $\beta$  source is inappropriate for the RV radioisotope battery. The RPV effect belongs to the indirect energy conversion mechanism, which can reduce the radiation damage effect of the energy conversion unit. As early as 1988, Prelas et al. proposed the concept of Nuclear-driven Flashlamps [8], and some studies on RPV effects have been followed [9,10]. However, the low conversion efficiency of RPV is also a problem [11–13]. Moreover, the performance of RV and RPV radioisotope battery in current research is difficult to meet the demand for the supply of miniaturized electronic devices.

In view of the preceding problems mentioned, this paper presents a multi-level isotope battery coupling mechanism between the RV and RPV effects of the  $\gamma$  radioisotope source. The  $\gamma$  rays, which are different from  $\alpha$  and  $\beta$  particles, cause less damage to the energy conversion materials. Butera et al. pioneered the use

\* Corresponding author at: Department of Nuclear Science and Engineering, Nanjing University of Aeronautics and Astronautics, Nanjing 211106, China.

E-mail address: [tangxiaobin@nuaa.edu.cn](mailto:tangxiaobin@nuaa.edu.cn) (X. Tang).

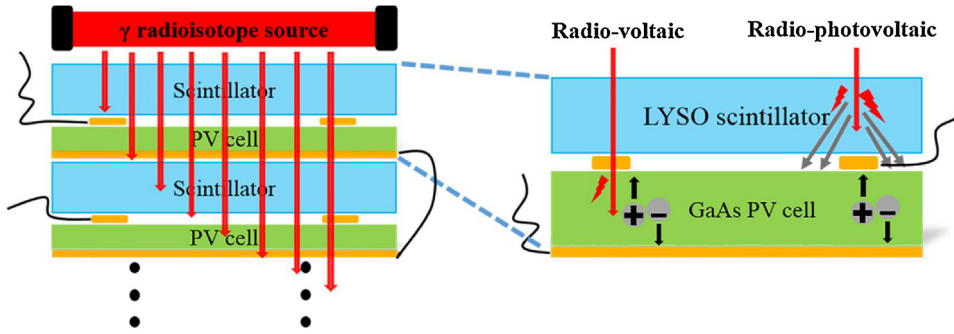


**Fig. 1.** Schematic of the dual effect multi-level isotope battery.

of  $^{55}\text{Fe}$  X-ray sources combined with GaAs photovoltaic (PV) cells, and obtained an open circuit voltage ( $V_{oc}$ ) of 0.265 V and a maximum output power ( $P_{max}$ ) of 0.0465 pW at  $-20\text{ }^{\circ}\text{C}$  [14]. Lee et al. proved the potential application value of  $\gamma$  rays on the RPV radioisotope battery [15,16]. Owing to the strong penetration principle of  $\gamma$  rays, the multi-level conversion module can combine the RV with RPV conversion mechanisms to realize the multi-level utilization of  $\gamma$  rays. Our previous works [17] have demonstrated the feasibility of using the scintillator to enhancing the performance of radioisotope battery. This study discusses the output characteristics of the two energy conversion mechanisms and presents an optimized design for the multi-level structure to improve the battery performance. The working principle of the multi-level isotope battery is shown in Fig. 1. In the multi-level isotope battery, a LYSO scintillator and a GaAs PV cell were coupled to form a conversion module with RV and RPV effects. The  $\gamma$  rays stimulate the scintillator to generate an enormous number of visible photons, which act on the PV cells to form an electrical output with RPV effect. Simultaneously, the  $\gamma$  rays directly act on the PV cells to form an electrical output through the RV effect. With the use of multi-level conversion module, the  $\gamma$  rays can be used step by step with the dual effects, and the isotope battery could produce a considerable output.

## 2. Monte Carlo simulation and theoretical analysis

### 2.1. Material selection

In this study, GaAs cell was selected as the energy conversion module for the RV and RPV effects. GaAs cell is a mature PV conversion unit with the band gap of 1.46 eV, which can produce high energy conversion efficiency and voltage output. The LYSO scintillator was used as the fluorescent material of the RPV effect. The LYSO scintillator have a good photon yield (approximately  $3.75 \times 10^4$  photons/MeV) and does not easily deliquesce in the air. At same time, the stability of LYSO scintillators is much higher than many other inorganic scintillators under high-energy radiation [18]. Such characteristics of the LYSO scintillator can ensure the stability of the isotope battery. Additionally, the emission wavelength of the LYSO scintillator is approximately 420 nm, which exactly matches the GaAs PV cell.

### 2.2. MCNP5 calculation model

A two-level conversion structure was selected as the research object in this study to investigate the output characteristics of the two kinds of conversion mechanisms in multi-level isotope battery. The detailed model of the two-level conversion structure was established by using the Monte Carlo simulation software, MCNP5. In the MCNP5 model, each LYSO scintillator was coupled to a GaAs PV cell to form a single-level conversion module. Each LYSO scintillator has a thickness of 5 mm that was divided into 20 layers with

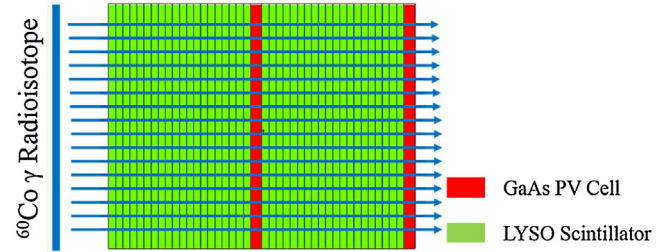


**Fig. 2.** Detailed structure model of the dual effect isotope battery established by MCNP5.

an area of  $1 \times 1\text{ cm}^2$ , and a density of  $7.1\text{ g/cm}^3$ . The GaAs PV cell model was set with a thickness of  $400\text{ }\mu\text{m}$ , an area of  $1 \times 1\text{ cm}^2$  and a density of  $5.89\text{ g/cm}^3$ . By using a plane unidirectional  $^{60}\text{Co}$  radioisotope source, the energy deposition behavior of decaying  $\gamma$  rays in LYSO scintillator and GaAs PV cell was calculated by using the \*F8 card.

### 2.3. Limit electrical output

Based on the MCNP5 simulation, a theoretical calculation model for the electrical output of the dual effect multi-level isotope battery was established, and the parameters of  $V_{oc}$ , short-circuit current ( $I_{sc}$ ),  $P_{max}$  and energy conversion efficiency ( $\eta$ ) for the multi-level isotope battery under the ideal conditions of  $10\text{ Ci}$   $^{60}\text{Co}$  radiation were obtained.

#### 2.3.1. Radio-photovoltaic effect

The RPV effect involves the energy conversion from decay energy to light energy and transformed to electricity energy. With the analysis of the induced fluorescence efficiency and the self-absorption of the scintillator, the electrical output from the RPV effect was obtained (Fig. 2).

According to the fluorescence process of the scintillator, the conversion efficiency of the  $\gamma$  energy deposited in the scintillator that converted into light energy can be expressed as follows [19]:

$$\eta = \eta_T \eta_S \eta_q \quad (1)$$

where  $\eta_T$  represents the efficiency of the exciton produced by the LYSO scintillator,  $\eta_S$  represents the efficiency of the exciton transferred to the luminescent center, and  $\eta_q$  represents the luminescent efficiency after the exciton is captured by the fluorescence center, which is equal to 1 under ideal conditions. For the LYSO scintillator,  $\eta_T$  and  $\eta_S$  can be expressed as follows [20]:

$$\eta_T = \frac{E_g}{2.67E_g + 0.87} \quad (2)$$

$$\eta_S = \frac{h\nu}{E_g} \quad (3)$$

**Table 1**

Calculated value of fluorescence conversion efficiency.

Parameter	$\eta_T$	$\eta_S$	$\eta$
Value	0.34	0.68	0.23

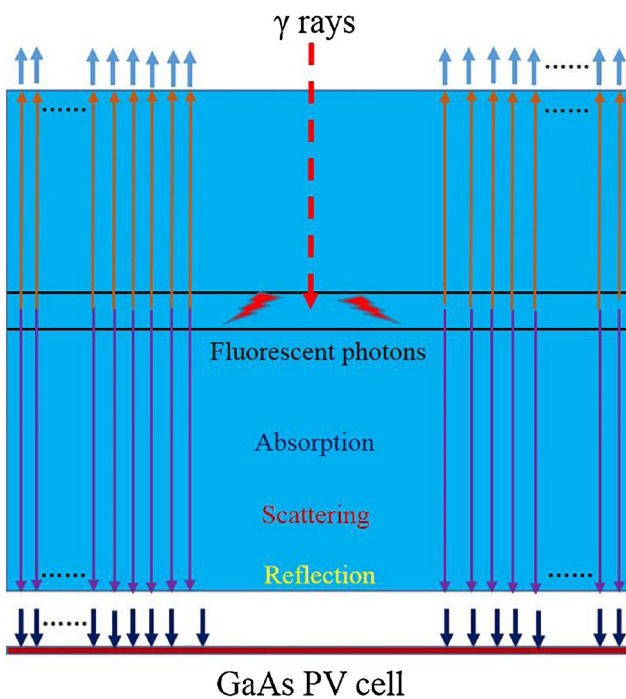


Fig. 3. Schematic of fluorescent photons transport in scintillator.

where  $E_g$  represents the band gap of the LYSO scintillator, which is approximately 3.3 eV, and  $h\nu$  is the photon energy that corresponds to the maximum emission wavelength of the LYSO scintillator. Table 1 shows the calculated values.

Considering the loss of absorption, scattering and reflection of the fluorescent photons transported in the scintillator material, a model of fluorescent photon transportation in the scintillator was established to calculate the fluorescence intensity on the surface of the scintillator, as shown in Fig. 3.

The generated fluorescent photons were assumed to be vertically emitted at both sides of the scintillator to simplify the calculation process, and their probability of emitting to each side was the same. The UV-vis fluorescence spectrophotometer (UV-2550, SHIMADZU) was used to measure scintillator transmissivity with different thicknesses to characterize the self-absorption effect of the LYSO scintillator (Fig. 4). The transmissivity of the scintillator can be expressed as:

$$T = \frac{I_t}{I_0} \quad (4)$$

where  $T$  represents the transmissivity of the scintillator,  $I_t$  represents transmitted light intensity, and  $I_0$  represents incident light intensity.

According to the Lambert-Beer law, the self-absorption coefficient  $\delta$  of fluorescent photons in the scintillator per unit thickness can be obtained as follows [21]:

$$\delta \propto \frac{\lg(1/T_l)}{l} \quad (5)$$

where  $l$  represents the thickness of the scintillator and  $T_l$  represents scintillator transmissivity at a thickness of  $l$ .

Considering the self-absorption effect, the surface fluorescence intensity generated by each scintillator layer was calculated and

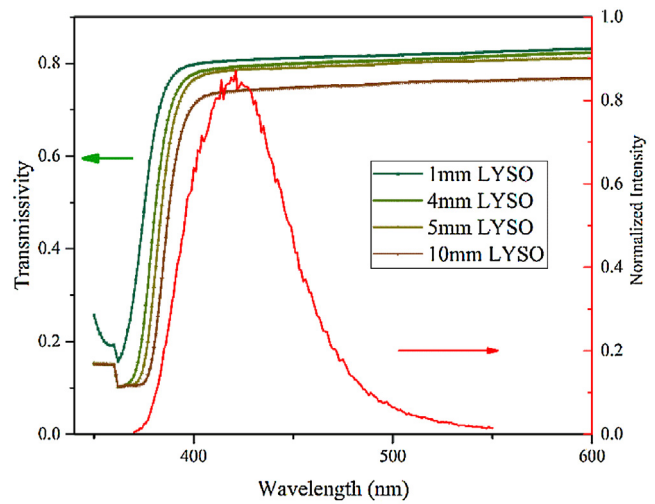


Fig. 4. Transmissivity with different thicknesses and emission spectra of LYSO scintillator.

summed to obtain the total surface emission fluorescence intensity as follows:

$$I = \sum_1^n I_i \quad (6)$$

where  $I$  is the total surface emission intensity,  $n$  is the number of layers in the MCNP5 model for the LYSO scintillator, and  $I_i$  is the surface emission intensity of the  $i$ -th layer in the MCNP5 model.  $I_i$  can be expressed as follows:

$$I_i = \frac{1}{2} I_{0,i} e^{-\delta l_i} \quad (7)$$

where  $I_{0,i}$  represents the fluorescence intensity generated in the  $i$ -th scintillator layer, and  $l_i$  represents the optical path length of the fluorescent photons produced by the  $i$ -th scintillator layer and transported to the surface.

The circuit current density generated by PV conversion can be obtained as follows [22]:

$$J(V) = J_{sc} - J_0 \left[ \exp \left( \frac{qV}{k_B T_a} \right) - 1 \right] \quad (8)$$

where  $J_{sc}$  represents short-circuit current density,  $J_0$  represents reverse saturation current density,  $k_B$  represent Boltzmann constant,  $T_a$  represents the environment temperature of 300 K, and  $q$  is the amount of electronic charge.  $J_{sc}$  and  $J_0$  can be expressed as follows:

$$J_{sc} = q \int_{E_g}^{\infty} b_s(E, T_a) dE \quad (9)$$

$$J_0 = q \int_{E_g}^{\infty} \frac{2F_a E^2}{h^3 c^2 [\exp(E/k_B T_a) - 1]} dE \quad (10)$$

where  $b_s(E, T_a)$  represents the density of the fluorescence photon spectrum, which can be obtained by the scintillator emission spectrum and the total surface emission intensity [23].  $h$  is Planck's constant,  $c$  is the speed of light in vacuum, and  $F_a$  is the environmental geometrical factor, which is equal to  $\pi$ .

Through the Shockley equation, the  $V_{oc}$  during PV conversion can be expressed as follows:

$$V_{oc} = \frac{k_B T_a}{q} \ln \left( \frac{J_{sc}}{J_0} + 1 \right) \quad (11)$$

The maximum output power density is expressed as follows:

$$P_{max} = J_{sc} V_{oc} FF \quad (12)$$

where  $FF$  represents fill factor, and its value can be calculated as follows [24]:

$$FF = \frac{v_{oc} - \ln(v_{oc} + 0.72)}{v_{oc} + 1} \quad (13)$$

where  $v_{oc}$  represents normalized open circuit voltage, which is the ratio of  $V_{oc}$  to  $kT/q$ .

### 2.3.2. Radio-voltaic effect

The  $\gamma$  rays directly interact with the GaAs PV cell and convert the decay energy into electrical energy through the RV effect. The electrical output generated by the RV effect was calculated based on the deposited energy of the  $\gamma$  rays in the GaAs PV cells.

In the calculation of the performance limit of the RV effect, all the energy deposited by the  $\gamma$  rays in the PV cell was assumed to be used to generate electron-hole pairs without any other loss.  $J_0$  and  $V_{oc}$  were calculated according to Eqs. (10) and (11). The  $J_{sc}$  generated by the RV effect can be expressed as follows:

$$J_{sc} = \frac{qE}{E_{ehp}} \quad (14)$$

$$E_{ehp} = 2.8E_g + 0.5 \quad (15)$$

where  $E$  represents the energy of the  $\gamma$  rays deposited in the GaAs PV cell,  $E_{ehp}$  represents the energy required to generate a pair of electron-hole pairs in the GaAs PV cell. The calculation of  $E_{ehp}$  (Eq. 15) was derived from the Klein formula. This empirical formula may have certain errors for some wide bandgap semiconductor materials [25,26], which may lead to slightly error in calculation results. In addition, the  $P_{max}$  of the RV effect was calculated by using Eq. (12).

### 2.3.3. Calculation results and analysis

**Table 2** shows the electrical output parameters generated by the two energy conversion mechanisms at each level of the conversion modules.

**Table 2** shows that the output performance of the first-level conversion module is higher than that of the second-level. According to the energy deposition features of  $\gamma$  ray in matter,  $\gamma$  ray deposits more energy into the first-level conversion module than that into the second-level, thereby resulting in a larger electrical output of the former than that of the latter. As shown in Fig. 5, the propor-

**Table 2**

Comparison of the output parameters produced by the two effects at each conversion module.

Serial number of conversion module	Energy conversion mechanism	$I_{sc}$ (mA)	$V_{oc}$ (V)	$P_{max}$ (mW)
1	RPV	0.161	0.8887	0.125
	RV	0.0844	0.872	0.0639
2	RPV	0.141	0.8853	0.109
	RV	0.0761	0.8694	0.0575

**Table 3**

Calculated output parameters of the dual effect isotope battery in series and in parallel.

	$I_{sc}$ (mA)	$V_{oc}$ (V)	$FF$	$P_{max}$ (mW)
Series	0.231	1.796	0.925	0.384
Parallel	0.463	0.898	0.872	0.363

tions of the performance parameters of the two energy conversion mechanisms in the second-level are close to those of the first-level. Moreover, all the electrical output parameters generated by the RPV effect are higher than those of the RV effect. However, the voltage output generated by the RV effect is very close to that generated by the RPV effect. The  $I_{sc}$  and  $P_{max}$  values of the RV effect reached approximately 0.5 times those of the RPV effect. The contribution of each effect on the battery performance cannot be ignored. Therefore, the RV and RPV effects should be both comprehensively considered during the optimization design of the multi-level conversion module.

During the calculation of the performance limit, the electron-hole pairs generated by the two effects were assumed to be collected completely, and the current and voltage were loss less both in the series and parallel. Under the irradiation of 10 Ci  $^{60}\text{Co}$  radioisotope source, the performance limit of the dual effect multi-level isotope battery was calculated when the multi-level conversion modules were connected in series and in parallel, as shown in **Table 3**.

As can be seen from **Table 3**, the multi-level conversion modules connected in series achieve larger output power than those connected in parallel. This finding may be attributed to the difference in internal resistance of the multi-level battery under the series and parallel connections. Beyond that, the multi-level con-

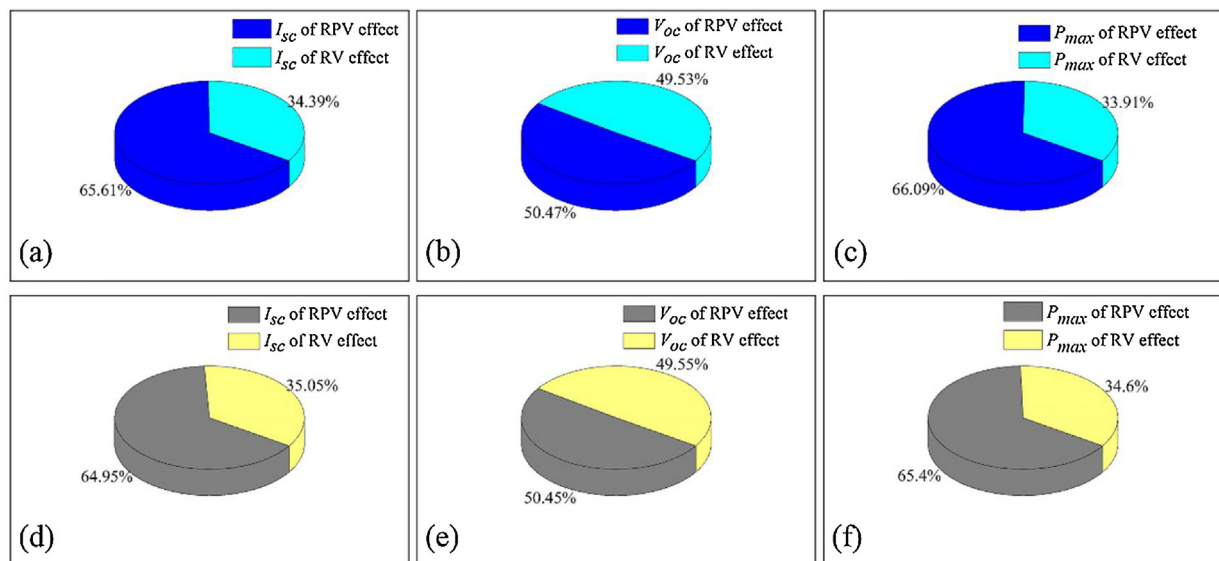


**Fig. 5.** (a), (b), and (c) represent  $I_{sc}$ ,  $V_{oc}$ , and  $P_{max}$  proportion of the two effects in the first-level conversion module, respectively; (d), (e) and (f) represent  $I_{sc}$ ,  $V_{oc}$ , and  $P_{max}$  proportion of the two effects in the second-level conversion module, respectively.

**Table 4**

Calculated energy conversion efficiency of the dual effect multi-level isotope battery.

	$P_{\text{source}}$ (mW)	$P_{\text{dep}}$ (mW)	$P_{\text{max}}$ (mW)	$\eta$	$\eta_{\text{total}}$
Series	74	12.83	0.384	2.99%	0.52%
Parallel	74	12.83	0.363	2.83%	0.49%

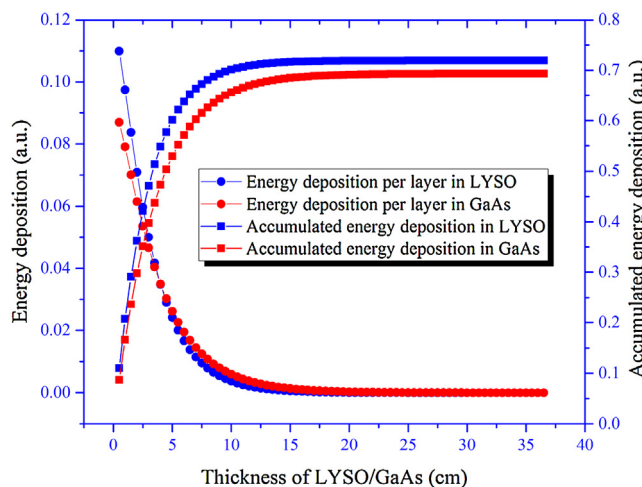


Fig. 6. Energy deposition of  $^{60}\text{Co}$   $\gamma$  rays in LYSO scintillator and GaAs PV cell, respectively.

version modules in series or parallel gain higher performance than the single first or second-level, as shown in the comparison results in [Tables 2 and 3](#).

The conversion efficiency of the multi-level isotope battery was characterized by calculating the total power of the  $^{60}\text{Co}$  radioisotope source and the deposited energy in the multi-level conversion module, as shown in [Table 4](#).  $P_{\text{source}}$  refers to the total power of 10 Ci  $^{60}\text{Co}$  source, and  $P_{\text{dep}}$  refers to the  $\gamma$  energy deposited into the conversion modules.  $\eta$  represents the energy conversion efficiency of the  $\gamma$  deposited energy converted into electrical energy, and  $\eta_{\text{total}}$  represents the conversion efficiency based on the total source power.  $\eta$  and  $\eta_{\text{total}}$  can be separately calculated as follows:

$$\eta = \frac{P_{\text{max}}}{P_{\text{dep}}} \quad (16)$$

$$\eta_{\text{total}} = \frac{P_{\text{max}}}{P_{\text{Source}}} \quad (17)$$

As presented in [Table 4](#), only 17.34% of the  $^{60}\text{Co}$   $\gamma$  rays energy were deposited into the multi-level conversion modules. This indicates that many  $\gamma$  rays passed through or backscattered in the conversion module and failed to deposit energy into it due to their strong penetration and Compton effects. Therefore, further improving the battery efficiency and output by increasing the number of conversion modules is an efficient way.

In the study of radioisotope batteries, the design of energy conversion module needs to focus on the range of scales that the ray interact with the energy conversion module [10,25]. In this work,  $\gamma$  rays emitted from  $^{60}\text{Co}$  has a large range in LYSO scintillator and GaAs PV cell. In order to estimate the appropriate scale size of conversion module, the MCNP5 was used to calculate the energy deposition of  $^{60}\text{Co}$   $\gamma$  rays in LYSO scintillator and GaAs PV cell, respectively ([Fig. 6](#)).

As the thickness of LYSO scintillator and GaAs PV cell increasing, the energy deposited therein gradually decreases. Accumulated energy deposition shows an upward trend with thickness increase and reaches a saturation value at 15–20 cm approximately. At a thickness of 20 cm, about 99.97% and 99.75% of  $\gamma$  ray energy were

deposited in LYSO scintillator and GaAs PV cell relative to saturation value, respectively. This can be used as a reference for the scale range when design the energy conversion module.

### 3. Experiment

#### 3.1. Preparation of multi-level conversion module

Two LYSO scintillators of 5 mm thickness and two GaAs PV cells produced by epitaxial growing were selected to prepare the multi-level module. One GaAs PV cell was bonded to the gold-plated PCB boards by using conductive silver paste and dried in a heating oven at 80 °C for 45 min to remove the organic solvent from the silver paste. An ultrasonic gold wire bonder was used to wire the front electrode lead to the gold-plated pad on the PCB. The leads were then soldered from the gold-plated pad and a single GaAs PV cell was formed. One 5 mm scintillator was loaded on the front of one GaAs PV cell, and then the first-level conversion module was formed. The other scintillator was loaded on the front of another GaAs PV cell to form the second-level conversion module. The scintillators were fixed by using foam glue. The first-level conversion module was placed on the front of the second-level module. Finally, a multi-level conversion module was assembled as shown in [Fig. 7](#). During the test, the multi-level conversion module was laid into a lead collimator to obtain collimated  $\gamma$  rays.

#### 3.2. Electrical performance measurement

The electrical performance of the multi-level isotope battery was measured at the  $^{60}\text{Co}$  Radiation Center of Nanjing University of Aeronautics and Astronautics. In the experiment, two dose rate sites of 0.103 kGy/h and 0.68 kGy/h were selected for the irradiation test. The  $I$ - $V$  characteristics of the dual effect multi-level isotope battery were measured by employing the Keithley 2636A multi-channel digital source. The 2636A digital source was placed outside the radioisotope chamber and linked to the battery sample through two long BNC signal transmission lines. The Labtrace 2.9 software was used to collect and process test data. [Figs. 8 and 9](#) show the diagrams of measurement principle and process, respectively.

#### 3.3. Measurement results and analysis

As shown in [Table 5](#), [Figs. 10 and 11](#), the performance parameters,  $I$ - $V$  curves and  $P$ - $V$  curves of the multi-level isotope battery under different experimental conditions were obtained, respectively. The maximum output power of the multi-level battery was 0.324  $\mu\text{W}$  under the dose rate of 0.68 kGy/h. The output parameters of the multi-level battery under high dose rates were evidently higher than those at low dose rates in series and in parallel. The series connection of the two-level conversion modules can enhance the  $V_{\text{oc}}$ , and the parallel connection can significantly improve the  $I_{\text{sc}}$ . Both cases can increase the output power of the battery. Therefore, using more conversion module connected with series or parallel could further improving the battery performance. Additionally, the  $P_{\text{max}}$  in series is higher than that in parallel, which is consistent with the preceding calculation results.

**Table 5**

Measured output parameters of dual effects isotope battery in series and in parallel.

Experimental conditions	$I_{\text{sc}}$ ( $\mu\text{A}$ )	$V_{\text{oc}}$ (V)	FF	$P_{\text{max}}$ ( $\mu\text{W}$ )
0.103 kGy/h-series	0.084	0.46	0.47	0.018
0.68 kGy/h-series	0.74	0.76	0.58	0.326
0.103 kGy/h-Parallel	0.12	0.19	0.45	0.0103
0.68 kGy/h-Parallel	1.38	0.36	0.54	0.268

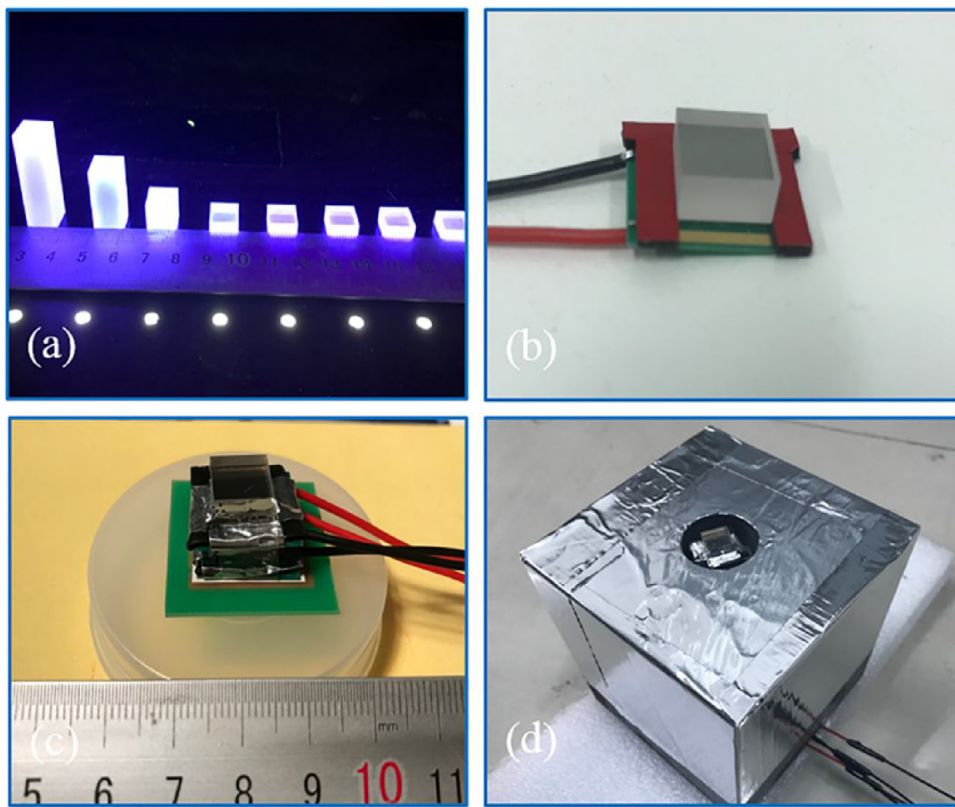


**Fig. 7.** Preparation process of the multi-level conversion module: (a) LYSO scintillator; (b) Single conversion module; (c) Multi-level conversion module; (d) Module in the lead can.

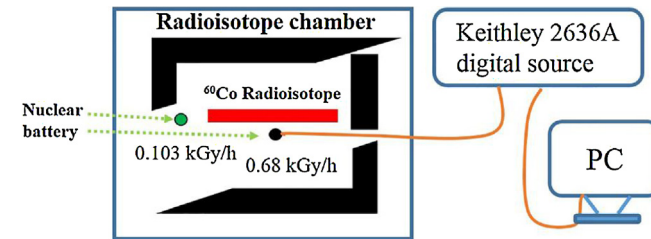


**Fig. 8.** Principle of measurement process.

**Table 6**

Energy conversion efficiency of multi-level isotope battery.

Experimental conditions	$P_{dep}$ (mW)	$P_{max}$ (μW)	$\eta$
0.103 kGy/h-series	0.21	0.018	0.0086%
0.68 kGy/h-series	1.386	0.326	0.0235%
0.103 kGy/h-Parallel	0.21	0.0103	0.0049%
0.68 kGy/h-Parallel	1.386	0.268	0.0193%

The energy deposited in the device per unit time has a positive correlation with the dose rates. With the higher dose rate irradiation, the more energy was deposited in the energy conversion module. A larger number carriers were generated by the RV and RPV effects, which makes the higher performance of  $I_{sc}$ ,  $V_{oc}$  and  $P_{max}$  under the higher dose rate.

This study estimated the energy conversion efficiency of the multi-level isotope battery to comprehensively understand the measured performance. The  $^{60}\text{Co}$  γ ray energy deposited into the multi-level conversion module of the battery was calculated based on dose rate. According to Eq. (16), the energy conversion efficiencies based on  $P_{dep}$  were obtained under different experimental conditions, as shown in Table 6. A high dose rate indicates a

high radioisotope source activity. The multi-level isotope battery obtained a higher  $\eta$  at high dose rate than that at low dose rate, which is well agree with the results in researches of betavoltaics effect and photovoltaic effect [27–30].

The equivalent circuit was used to analyzing the physical mechanism of the various efficiency. Fig. 12. shows the equivalent circuit of the battery under ideal conditions. Where  $R_s$  represents the series resistance,  $R_{sh}$  represents the shunt resistance,  $I_0$  represents the reverse saturation current,  $I_p$  represents the excitation current,  $I$  represents the actual current.

With the increase of the incident light intensity, the  $R_{sh}$  in the device increases accordingly, and both  $R_s$  and  $I_0$  will decrease [30]. The  $R_s$ ,  $R_{sh}$  and  $I_0$  greatly affect the output performance of battery. The increase of  $R_{sh}$  and the decrease of  $R_s$  reduce the power loss caused by the internal resistance of the battery (Eq. (18)), thereby increasing the energy conversion efficiency (Eq. (20)). The decrease of  $I_0$  is beneficial to increase the  $V_{oc}$  of the battery (Eq. (19)).

$$P_{loss} = \left( 1 + \frac{R_s}{R_{sh}} \right) I^2 R_s \quad (18)$$

where  $P_{loss}$  represents the power loss caused by the internal resistance.

$$V_{oc} = \frac{k_B T_a}{q} \ln \left( \frac{I_{sc}}{I_0} + 1 \right) \quad (19)$$

$$\eta = \frac{P_{max}}{P_{max} + P_{loss}} \quad (20)$$

As the dose rate increases, the greater quantity of light intensity were generated by the interaction of the gamma ray and the scintillator. As analyzed above, with the increasing of light intensity, the  $R_{sh}$  of the GaAs photovoltaic module increase,  $R_s$  and  $I_0$  decreases, which made the  $P_{loss}$  decreases (Eq. 18). Thereby the conversion efficiency of the battery was improved (Eq. 20). This is the reason

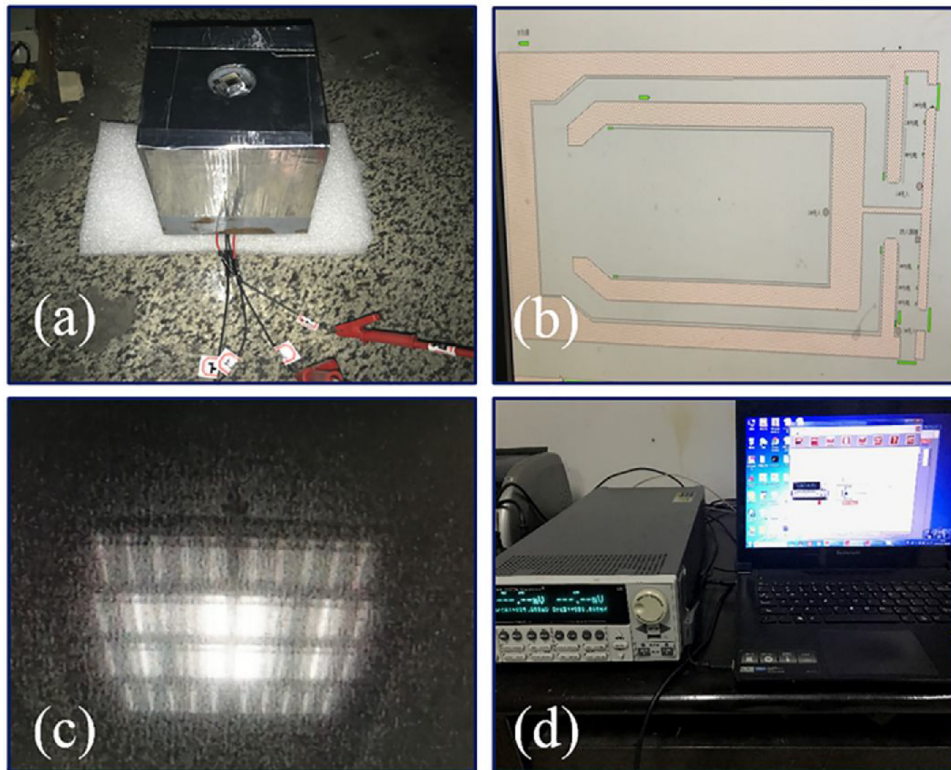


**Fig. 9.** Measurement process: (a) Placement of the multi-level isotope battery in the  $^{60}\text{Co}$  chamber; (b)  $^{60}\text{Co}$  chamber structure; (c)  $^{60}\text{Co}$  radioisotope; (d) Measurement system.

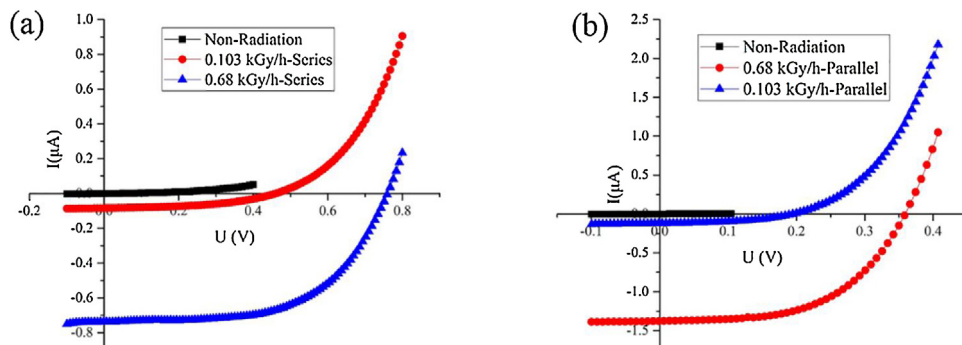


**Fig. 10.** (a)  $I$ - $V$  curve of multi-level isotope battery with different dose rates in series; (b)  $I$ - $V$  curve of multi-level isotope battery with different dose rates in parallel.

why the battery get higher energy conversion efficiency at high dose rates.

Considering the shielding of the lead collimator during the actual measurement process, the isotope battery was irradiated with a dose rate below the measured value. That means the calculated conversion efficiency could be underestimated.

The preceding experimental results show that the use of multi-level energy conversion modules for realizing the dual utilization of  $\gamma$  ray energy is feasible. Although the conversion efficiency is low, but it can optimize the multi-level structure to increase the utilization of  $\gamma$  rays. In addition, the battery performance was significantly increased at a high dose rate, indicating that the performance of battery can be further enhanced by using high activity sources coupled with additional conversion modules.

In addition, the limit output performance of multi-level battery at 0.103 kGy/h and 0.68 kGy/h were calculated by using the methods of Section 2.3, respectively. Table 7 shows the results of the theoretical calculation.

**Table 7**  
Calculated electrical performance of multi-level isotope battery.

Experimental conditions	$P_{dep}$ (mW)	$I_{sc}$ ( $\mu\text{A}$ )	$V_{oc}$ (V)	$P_{max}$ ( $\mu\text{W}$ )	$\eta$
0.103 kGy/h-series	0.21	0.0409	1.3492	0.0501	0.0239%
0.68 kGy/h-series	1.386	0.274	1.4476	0.3543	0.0256%
0.103 kGy/h-Parallel	0.21	0.0819	0.6746	0.0465	0.0221%
0.68 kGy/h-Parallel	1.386	0.549	0.7238	0.337	0.0243%

From the Tables 5–7, the result of the experiment is slightly lower than the theoretical calculation. The reason is that there are some ideal assumptions when calculation the output of the battery by using the methods of Section 2.3. As shown in Table 7, the performance of the battery was greatly improved with increasing the dose rate. The  $P_{max}$  and  $\eta$  in series is higher than that in parallel. All those results of theoretical calculation shows the same trend as the experiment.

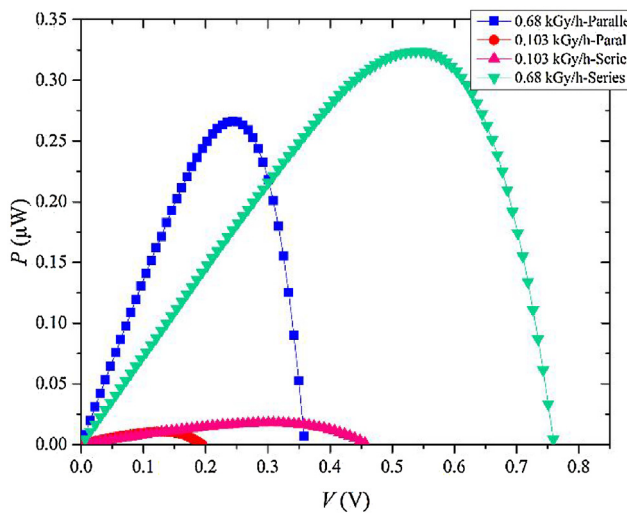


**Fig. 11.**  $P$ - $V$  curve of multi-level isotope battery with different dose rates in series and in parallel.

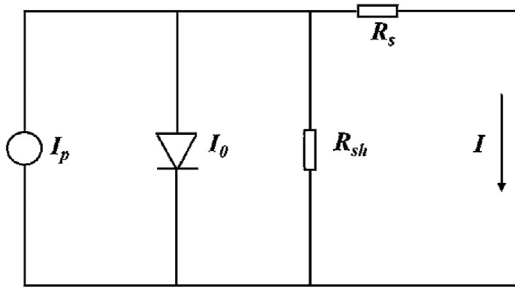


**Fig. 12.** The equivalent circuit of the battery.

#### 4. Optimization design

The calculated and measured results were both based on certain structural parameters, including the thicknesses of the GaAs PV cell and the LYSO scintillator. The selected LYSO scintillator was thicker than the GaAs PV cell. Therefore, the former played a crucial role in the energy deposition behavior of the  $^{60}\text{Co}$   $\gamma$  source and the consequent performance of the multi-level isotope battery. As the thickness of the LYSO scintillator changes, the energy deposited in the scintillator changes accordingly, thereby resulting in the change of the output parameters produced by the RV and the RPV effects. Adjusting the thickness of the LYSO scintillator to maximize the electrical output generated by both energy conversion mechanisms is necessary to optimize the structure.

Taking the first-level conversion module as an example, the output performances of the first-level conversion module were discussed under LYSO scintillators of different thicknesses by using the familiar method in Section 2 to facilitate the analysis. The thicknesses of the LYSO scintillator were set to 0.1, 0.5, 1, 1.5, 2, 2.5, 3, 3.5, 4, 4.5, 5, 5.5, and 6 cm. Fig. 13 shows the calculated output parameters.

The electrical output parameters all increased and then decreased with the increasing of the LYSO thickness. When the LYSO thickness was 1.5 cm, the  $I_{sc}$ ,  $V_{oc}$  and  $P_{max}$  of the first-level conversion module reached maximum values. The contributions of the RV and RPV effects on the output parameters of the first-level module were calculated and analyzed with the LYSO scintillator of various thicknesses and the results are shown in Figs. 14–16.

The calculation results show that the values of  $I_{sc}$ ,  $V_{oc}$  and  $P_{max}$  generated by the RPV effect increased and then decreased as the

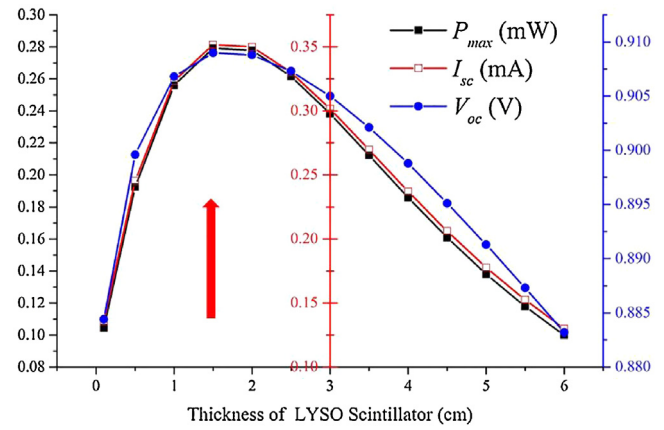


**Fig. 13.** Regular pattern of output parameters with the change of LYSO scintillator thickness.

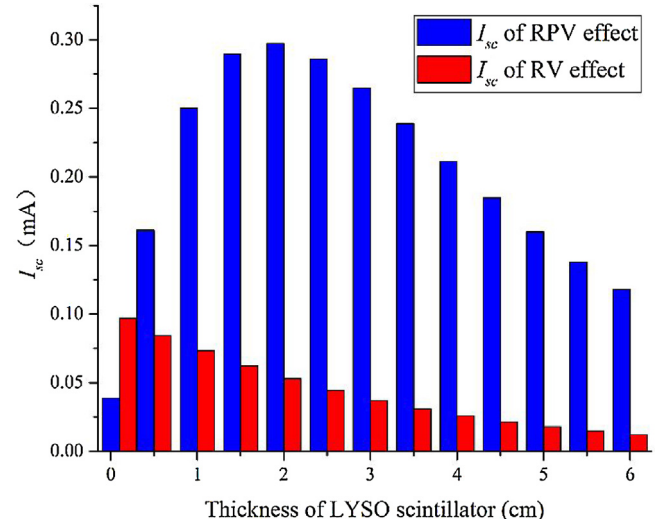


**Fig. 14.**  $I_{sc}$  of RV and RPV effects with different LYSO scintillator thicknesses.

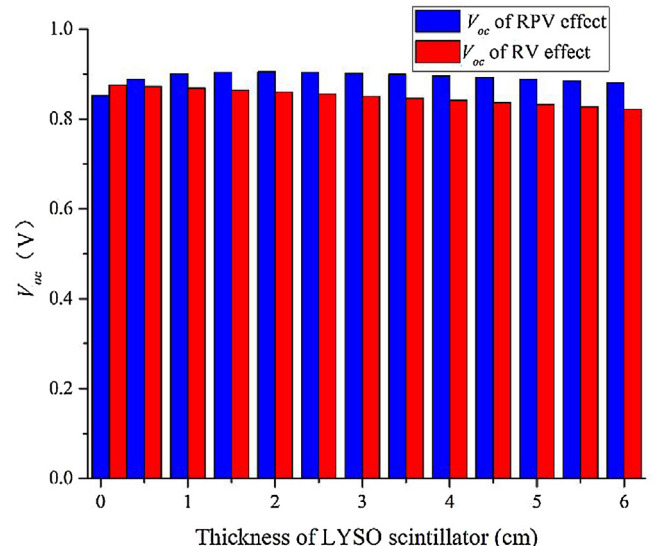


**Fig. 15.**  $V_{oc}$  of RV and RPV effects with different LYSO scintillator thicknesses.

LYSO thickness increased and reach their peaks when the thickness was 2 cm. As the thickness of LYSO increased from 0.1 cm to 2 cm, the energy deposited in the scintillator gradually increased. At this time, the self-absorption effect on fluorescence was small, and

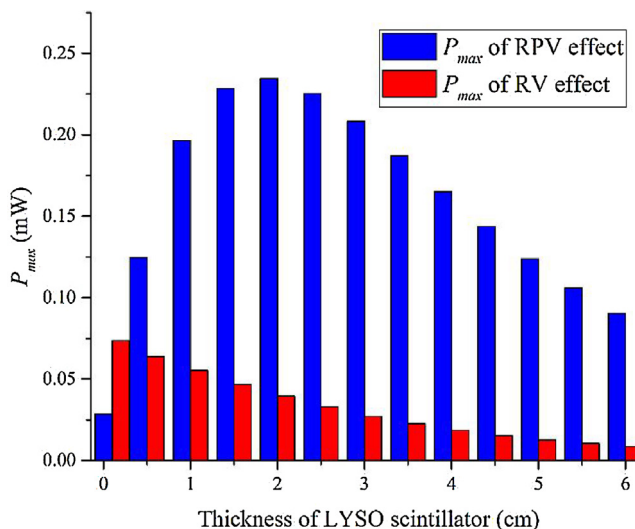


Fig. 16.  $P_{max}$  of RV and RPV effects with different LYSO scintillator thicknesses.

the surface emission intensity showed an upward trend, thereby resulting in the enhancement of the RPV effect. When the thickness of LYSO exceeded 2 cm, the self-absorption effect increased. This phenomenon led to the gradual decrease of the total surface emission intensity and the reduction of the RPV effect. As the thickness of the scintillator increased, the blocking effect of the scintillator reduced the energy deposition of  $\gamma$  rays in GaAs PV cell. This reduction weakened the contribution of the RV effect, thereby resulting in the decrease of  $I_{sc}$ ,  $V_{oc}$  and  $P_{max}$ .

The preceding results demonstrate that optimizing the thickness of the LYSO scintillator is an effective way for optimizing the dual effect of the multi-level isotope battery. The influence of the LYSO thickness on the RPV effect is quite different from that on the RV effect. This finding shows that the competition between the two kinds of conversion mechanisms should be comprehensively considered in the optimization design of the multi-level isotope battery. In addition, the optimization of the GaAs thickness and the multi-level modules should be studied in the future.

## 5. Conclusion

This work proposed a multi-level isotope battery with RV/RPV dual effects based on  $^{60}\text{Co}$   $\gamma$  source. The MCNP5 calculations showed that limit performance of  $P_{max}$  reached 0.384 mW and  $\eta_{total}$  was 0.52% under the irradiation of 10 Ci  $^{60}\text{Co}$  in series. The results revealed that the RPV effect produced more electrical output than the RV effect, but the contribution of each effect on the battery was significant.

The dual effect multi-level isotope battery was prepared and measured with the irradiation of  $^{60}\text{Co}$  source. The  $P_{max}$  and  $\eta$  of the multi-level battery reach 0.326  $\mu\text{W}$  and 0.0235% under the dose rate of 0.68 kGy/h. As predicted, the output power of the battery with multi-level conversion modules in series was better than that in parallel. The experimental results demonstrate the feasibility of the dual effect multi-level isotope battery based on  $\gamma$  radioisotope source. The performance of the isotope battery can be significantly enhanced by using high activity source coupled with additional conversion modules.

Taking the first-level conversion module as an example, the structure of the multi-level isotope battery was optimized by using MCNP5. The electrical performance increased and then decreased with the increasing of the scintillator thickness. When the LYSO scintillator was 1.5 cm, the  $I_{sc}$ ,  $V_{oc}$  and  $P_{max}$  of the first-level conversion module reached their maximum values. The optimization

design of multi-level structure needs to comprehensively consider the competitive relationship between the RV and RPV mechanisms.

The following work should increase the number of conversion modules to improve the performance of the dual effect isotope battery. Meanwhile, the optimization of the GaAs thickness and the multi-level modules should be further studied in the future.

## Acknowledgements

This work was supported by the National Natural Science Foundation of China (Grant No. 11675076 and 11505096), the Natural Science Foundation of Jiangsu Province (Grant No. BK20150735), the Shanghai Aerospace Science and Technology Innovation Project (Grant No. SAST2016112), the Foundation of Graduate Innovation Center in NUAA (Grant No. kfjj20170603), and the Priority Academic Program Development of Jiangsu Higher Education Institutions.

## References

- [1] J. Blanchard, D. Henderson, A. Lal, A nuclear microbattery for MEMS devices, *Off. Sci. Tech. Inf. Tech. Reports* (2002) 3.
- [2] F. Rahmani, H. Khosravinia, Optimization of silicon parameters as a betavoltaic battery: comparison of Si p-n and Ni/Si Schottky barrier, *Radiat. Phys. Chem.* 125 (2016) 205–212.
- [3] K. Zhang, G. Gui, P. Pathak, J.H. Seo, J.P. Blanchard, Z. Ma, Quantitative modeling of betavoltaic microbattery performance, *Sens. Actuators A Phys.* 240 (2016) 131–137.
- [4] T. Wacharasindhu, B.R. Nullmeyer, J.W. Kwon, J.D. Robertson, A.Y. Garnov, Mechanisms leading to losses in conventional betavoltaics and evolution: utilizing composite semiconductor with infused radioisotope for efficiency improvement, *J. Microelectromech. Syst.* 23 (2014) 56–65.
- [5] Y. Chang, C. Chen, P. Liu, J. Zhang, A betavoltaic microcell based on Au/s-SWCNTs/Ti Schottky junction, *Sens. Actuators A Phys.* 215 (2014) 17–21.
- [6] M. Lu, G.G. Zhang, K. Fu, G.H. Yu, D. Su, J.F. Hu, Gallium nitride schottky betavoltaic nuclear batteries, *Energy Convers. Manag.* 52 (2011) 1955–1958.
- [7] S.T. Revankar, T.E. Adams, Advances in betavoltaic power sources, *J. Energy Power Sources* 1 (2014) 321–329.
- [8] M.A. Prelas, F.P. Boody, G.H. Miley, J.F. Kunze, Nuclear driven flashlamps, *Laser Part. Beams*, 6 (1988) 25–62.
- [9] M.A. Prelas, E.J. Charlson, E.M. Charlson, J. Meese, G. Popovici, T.B.T.-I.C. on the A. of D.F. and R.M. Stacy, *Diamond Photovoltaics In Energy Conversion*, 1993.
- [10] M.A. Prelas, C.L. Weaver, M.L. Watermann, E.D. Lukosi, R.J. Schott, D.A. Wisniewski, A review of nuclear batteries, *Prog. Nucl. Energy.* 75 (2014) 117–148.
- [11] Z.H. Xu, X.B. Tang, Y.P. Liu, Z.R. Zhang, W. Chen, Z.C. Yuan, K. Liu, ZnS:cu phosphor layers as energy conversion materials for nuclear batteries: a combined theoretical and experimental study of their geometric structure, *Energy Technol.* 5 (2017) 1638–1646.
- [12] J. Russo, M. Litz, I.I. William Ray, B. Smith, R. Moyers, A radioluminescent nuclear battery using volumetric configuration:  $^{63}\text{Ni}$  solution/ZnS:Cu,Al/InGaP, *Appl. Radiat. Isot.* 130 (2017) 66–74.
- [13] A. Sharma, J.M. Melancon, S.G. Bailey, S.R. Zivanovic, Betavoltaic cells using P3HT semiconductive conjugated polymer, *IEEE Trans. Electron. Devices* 62 (2015) 2320–2326.
- [14] S. Butera, M.D. Whitaker, G. Lioliou, A.M. Barnett, AlGaAs  $^{55}\text{Fe}$  x-ray radioisotope microbattery, *Sci. Rep.* 6 (2016) 38409.
- [15] H. Lee, M.S. Yim, Examination of spent fuel radiation energy conversion for electricity generation, *Nucl. Eng. Des.* 300 (2016) 384–392.
- [16] H. Lee, M.S. Yim, Examination of scintillator-photovoltaic cell-based spent fuel radiation energy conversion for electricity generation, *Prog. Nucl. Energ.* 94 (2017) 46–54.
- [17] Z.R. Zhang, X.B. Tang, Y.P. Liu, Z.H. Xu, Z.C. Yuan, K. Liu, W. Chen, GaAs radiovoltaic cell enhanced by  $\text{Y}_2\text{Si}_5\text{O}_9$  crystal for the development of new gamma microbatteries, *Nucl. Instrum. Meth. B*, 398 (2017) 35–41.
- [18] C. Hu, F. Yang, L. Zhang, R.Y. Zhu, J. Kapustinsky, R. Nelson, Z. Wang, Proton-Induced radiation damage in BaF<sub>2</sub>, LYSO and PWO crystal scintillators, *IEEE Trans. Nucl. Sci.* 60 (2018) 1.
- [19] L.L. Xu, C.T. Sun, D.F. Xue, Recent advances in rare earth scintillation crystals, *Sci. Sin.* 46 (2016) 657–673.
- [20] K.E. Bower, *Polymers, Phosphors, and Voltaics for Radioisotope Microbatteries*, CRC Press, 2002.
- [21] H. Yuan, Measurement of average light attenuation coefficient of plastic scintillators, *Nucl. Electron. Detect. Technol.* 2 (1982) 19–26.
- [22] J. Nelson, *The Physics of Solar Cells*, vol. 57, Imperial college press, 2003, pp. 384.
- [23] L. Hong, X.B. Tang, Z.H. Xu, Y.P. Liu, D. Chen, Radioluminescent nuclear batteries with different phosphor layers, *Nucl. Instrum. Methods Phys. Res.* 338 (2014) 112–118.

- [24] X.B. Tang, Y.P. Liu, D. Ding, D. Chen, Optimization design of GaN betavoltaic microbattery, *Sci. China Tech. sci.* 55 (2012) 659–664.
- [25] M. Prelas, M. Boraas, F.D.L.T. Aguilar, J.D. Seelig, M.T. Tchouaso, D. Wisniewski, *Nuclear Batteries and Radioisotopes*, Springer International Publishing, 2016.
- [26] P.J. Sellin, J. Vaitkus, New materials for radiation hard semiconductor detectors, *Nucl. Instr. And Meth. A* 557 (2006) 479–489.
- [27] Y.P. Liu, X.B. Tang, Z.H. Xu, L. Hong, H. Wang, M. Liu, D. Chen, Influences of planar source thickness on betavoltaics with different semiconductors, *J. Radioanal. Nucl. Chem.* 304 (2015) 517–525.
- [28] H. Guo, Y. Shi, Y. Zhang, Y. Zhang, J. Han, Fabrication of SiC p-i-n betavoltaic cell with  $^{63}\text{Ni}$  irradiation source, *Electron. Devices Solid-state Circuits* (2011) 1–2.
- [29] D.J. Mbewe, H.C. Card, D.C. Card, A model of silicon solar cells for concentrator photovoltaic and photovoltaic/thermal system design, *Sol. Energy* 35 (1985) 247–258.
- [30] F. Khan, S.N. Singh, M. Husain, Effect of illumination intensity on cell parameters of a silicon solar cell, *Sol. Energy Mater. Sol. Cells.* 94 (2010) 1473–1476.

## Biographies



**Xiao Guo** received the BEng degree in nuclear engineering and nuclear technology from the University of South China, in 2016. He is a master candidate in nuclear technology and materials engineering at Nanjing University of Aeronautics and Astronautics. His research interests are focused on radiation energy conversion mechanism, and his current research interests are design and preparation of new isotope battery.



**Yunpeng Liu** received his BSc degree in applied physics from Nanjing University of Aeronautics and Astronautics, in 2009. He received his PhD degree in nuclear technology and materials engineering from the same university, in 2014. He is currently working at Department of Nuclear Science and Engineering at Nanjing University of Aeronautics and Astronautics as a lecturer. He presided research projects supported by the National Natural Science Foundation of China, the Natural Science Foundation of Jiangsu Province, China Postdoctoral Science Foundation. He has published 10 papers related to his research. He holds and has licensed 7 patents. His current research interests are application of Monte Carlo method in particle transport, design and preparation of new isotope battery, and space laser/X-ray coupled communication technology.



**Zhiheng Xu** received the BEng degree in nuclear engineering and nuclear technology from East China University of Technology, in 2012. Since then, Zhiheng is an MD-PhD candidate majored in nuclear technology and materials engineering at Nanjing University of Aeronautics and Astronautics. His research interests are radiation energy conversion mechanism and nuclear battery technology. As a PhD student, he is focused on the development and fabrication of radioluminescent nuclear batteries as well as theory and potential applications of new semiconductor and nano-sized fluorescent material.



**Zhangang Jin** received the BEng degree in nuclear engineering and nuclear technology from Yantai University, in 2016. He is master candidate in nuclear technology and application at Nanjing University of Aeronautics and Astronautics. His research interests are focused on radiation energy conversion mechanism, and his current research interests are design and preparation of new isotope battery.



**Kai Liu** received the BEng degree in nuclear reactor engineering from University of South China, in 2015. He is a MD candidate in nuclear technology and applications engineering at Nanjing University of Aeronautics and Astronautics. His current research interests are mechanism and practical design of nuclear batteries and exploring more energy conversion mechanisms to convert radioactive decay energy into electrical energy.



**Zicheng Yuan** received the BEng degree in radiation protection and environmental engineering from Chengdu University of Technology, in 2015. He is researching his PhD in nuclear technology and materials engineering at Department of Nuclear Science and Engineering at Nanjing University of Aeronautics and Astronautics. His research interests are currently focused on radiation thermoelectric conversion device design, thermophotovoltaic converter design for radioisotope power systems.



**Pin Gong** received his BEng degree in nuclear physics and nuclear technology engineering from Nanjing University, in 2002. He received his MBA degree in MBA center of Nanjing University of Finance and Economics in 2013. He worked in the Department of Nuclear Science and Engineering of Nanjing University of Aeronautics and Astronautics from 2002. He is researching his PhD in nuclear technology and materials engineering at Department of Nuclear Science and Engineering at Nanjing University of Aeronautics and Astronautics. His research interests are currently focused on radiation detection and nuclear instruments.



**Xiaobin Tang** received his BEng degree in materials science and engineering from Nanjing University of Aeronautics and Astronautics, in 2000. He received his PhD degree in measuring and testing technologies and instruments from the same university, in 2009. He is now a professor in Department of Nuclear Science and Engineering at Nanjing University of Aeronautics and Astronautics. He is China Nuclear Society Radiation Physics Branch; Jiangsu Provincial Biomedical Engineering Society of medical physics professional committee deputy secretary-general, standing committee. He presided over the national level, provincial and ministerial level and other research projects more than 30 items. Tang has published over 60 journal papers and 20 patents (11 authorized) in nuclear technology and other disciplines in the field of research work, such as nuclear materials, nuclear medicine, nuclear instrument, etc. Tang's research interests include radiation energy conversion mechanism and nuclear battery technology, material irradiation effect and new materials for nuclear use, new technique and dose effect of radiation therapy, radiation detection imaging and nuclear instrument development, and space radiation physics and nuclear technology application.